New Luminescent Metal–Organic Frameworks

Trabajo de Fin de Máster

Máster Interuniversitario en Nanociencia y Nanotecnología Molecular

Universidad de La Laguna, septiembre de 2018

Autora:
Carla Varela Núñez

Directores:
Dr. Jorge Pasán García
Dra. Catalina Ruiz Pérez

Abstract

The present master thesis entitled *New Luminescent Metal-Organic Frameworks* focuses on the synthesis and characterization of several new metal–organic frameworks (MOFs), which are a kind of organic-inorganic hybrid compounds with one-, two-, or three-dimensional structural topologies consisting of inorganic metal ions/clusters and organic ligands. The relevance of the new MOFs synthesized dwells in the luminescence properties that they exhibit.

The construction of new MOFs has been rapidly developed in recent years, not only due to their interesting molecular topologies and crystal packing motifs but also due to their potential applications as functional materials. MOFs can be readily synthesized from the self-assembly of metal ion nodes with organic ligands. Multi-carboxylic acids have been widely used to synthesize high dimensional frameworks. In particular, 1,2,4,5-benzenetetracarboxylate is a versatile ligand that leads to numerous different coordination polymers with lanthanide ions.

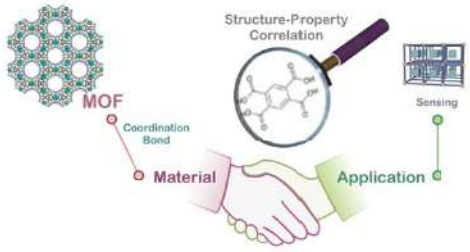

Figure 1: *MOFs: from synthesis to applications.*

Among the wide variety of properties of interest that a given material can exhibit, luminescence is attracting an increasing attention due to its potential application in optical devices for lighting equipment and optical storage,

optical switching, and sensing. At this respect, luminescent metal–organic frameworks (LMOFs) are a quickly growing class of crystalline materials with great potential for use across a broad range of applications. The lanthanide elements, which possess partially filled 4f orbitals, can form coordination polymers that exhibit various coordination geometries even with the same ligand.

An extensive work has been carried out using 1,2,4,5-benzenetetracarboxylic acid (H_4bta) as ligand and 1,2-di(4-pyridyl)-ethylene (bpe), 1,2,4-triazole (tz), imidazole (im) and 4,4'-azobis(pyridine) (azpy) in order to perform cation exchanges. Several lanthanide coordination polymers with good luminescence properties have been synthesized by hydrothermal method, and an investigation on the formation of lanthanide coordination compounds based on the use of cation exchange has also been performed. The seven LMOFs prepared are, specifically: [Ln(bta)][$(CH_2)_2NH_2$] (Ln=Tb (**1**), Ln=Pr (**2**)), [Ln(bta)]$_2$(bpe) (Ln= Tb (**3**), Ln=Pr (**4**)), [Tb(bta)](im) (**5**), [Tb(bta)]$_2$ (azpy) (**6**), and [Tb(bta)](tz) (**7**).

Single-crystal X-ray diffraction reveals that complex **1** crystallizes in the to orthorhombic space group $P2_12_12_1$, while complexes **2** and **3** in the triclinic space group P-1. The Pr-complexes obtained are isostructural as deduced by means of single crystal and powder X-ray diffraction analysis, unlike Tb-complexes, which are found to possess different crystal structures. Luminescence measurements reveal that the Tb^{3+} compounds exhibit several strong characteristic emission bands for isolated Tb^{3+} ions in the visible region when excited between 320 and 375 nm; similarly, the Pr^{3+} compounds display the characteristic emission bands for isolated Pr^{3+} ions.

Contents

Chapter 1

Introduction

The present report is structured in four chapters. In this first chapter, the work that has been carried out during this Master's degree is presented and justified. The aim of this project and the objectives to achieve are detailed, along with the reason why the materials synthesized and studied belong to a field of scientific interest. Also, the theoretical background surrounding the main theme of the project is discussed.

1.1 Motivation and objectives

Due to their structural and functional tunability as well as their ever-expanding application scope, metal–organic frameworks have become one of the most fascinating classes of materials for both scientists and engineers [1]. Additionally, the study of lanthanide complexes is an attractive area of research because of the special configuration of 4f electrons and the variable coordination numbers of lanthanide elements, which may form compounds with applications in electronics, magnetism, optics, medicine, chemistry, and biology [2]. Recently, lanthanide metal-organic frameworks have received much attention: the combination of lanthanoid(III) ions with carboxylate–containing bridging ligands has produced a great variety of extended metal–

organic frameworks (MOFs) which are of special importance since they exhibit interesting properties such as porosity, luminescence, magnetism, and catalytic activity [3].

With this in mind, the main purpose of this project consists on the synthesis of several lanthanide MOFs. The characterization of each one of them to find out their crystal structure, composition and luminescence properties is therefore another significant objective to achieve. The compounds synthesized and studied are, specifically: [Ln(bta)][$(CH_2)_2NH_2$] (Ln=Tb (**1**), Ln=Pr (**2**)), [Ln(bta)]$_2$(bpe) (Ln= Tb (**3**), Ln=Pr (**4**)), [Tb(bta)](im) (**5**), [Tb(bta)]$_2$ (azpy) (**6**), and [Tb(bta)](tz) (**7**).

Thereby, the goals to be attained can be summarized as follows:

1. Preparation of metal-organic frameworks via two different synthetic routes: hydrothermal synthesis and cation exchange.

2. Description and characterization of the resulting complexes by various techniques, such as XRD (X-ray diffraction), IR spectra measurements, mass spectrometry and elemental analysis.

3. Study of the luminescence properties that these materials exhibit.

1.2 State of the art

1.2.1 Metal-Organic Frameworks

Metal–organic frameworks (MOFs) are a class of functional materials constructed by the combination of organic linkers and metal ions to produce extended networks that possess pores and cavities of adjustable size and shape [4]. Following the IUPAC recommendation, MOFs are classified as coordination polymers (or alternatively coordination networks) with open framework

structures containing potential voids [5]. These materials are formed by reticular synthesis, which creates strong bonds between metal-containing units (secondary building units, SBUs) and organic linkers, creating open crystalline frameworks with permanent porosity [6]. This crystallinity allows X-ray diffraction techniques to provide exact structural information about MOFs [7]. Moreover, they maintain their underlying structure and crystalline order upon expansion of the organic units and inorganic SBUs, which greatly widens the scope of this chemistry [4].

The appropriate selection of the organic linker together with a rational synthetic route can be used to modulate structural diversity. Among the different organic ligands, those containing carboxylate groups are often selected due to their abundant coordination modes, which allow the occurrence of different structural topologies, along with the ability of the carboxylate group to act as a hydrogen-bond acceptor and/or donor, which can help to stabilize the crystal structure [8]. The organic ligands often contain aromatic or conjugated π moieties that are subject to excitation, giving rise to optical emission or photoluminescence (PL) upon irradiation. In addition, the metal components can also contribute to photoluminescence, in which case lanthanides or various inorganic clusters are often involved [9].

In particular, 1,2,4,5-benzenetetracarboxylic acid (H_4bta) is a versatile building block for the architectures of polymeric structures due to its variety of bridging abilities, and its high symmetry is also helpful for the growth of crystals [10]. Investigations about the coordination chemistry of this ligand after total or partial deprotonation show the high versatility towards transition metals and lanthanide ions [11].

Luminescent Metal-Organic Frameworks

A very interesting and well-investigated topic about MOFs is their optical emission properties and related applications [9], such as fluorescent sensors, nonlinear optics, photocatalysis, electroluminescent devices, biomedical imaging, and drug delivery monitoring and treatment among others [12, 13]. Luminescent metal–organic frameworks (LMOFs) are an important and rapidly growing sub-category of MOFs in which photon emission arises following the absorption of radiative excitation energy [7].

Luminescence can broadly be defined as the emission of light occurring from excited electronic states, which is preceded by the absorption of energy [7]. In particular, photoluminescence embraces two different kinds of light emission: *fluorescence* and *phosphorescence*. *Fluorescence* is caused by irradiation with light (normally visible or UV), normally occurs within nanoseconds to milliseconds after irradiation, and involves the excitation of electrons into states with a higher energy, from where radiative decay is possible. Typically, the emitted wavelengths are longer than the excitation ones; otherwise one speaks of *upconversion fluorescence*. In contrast, *phosphorescence* is a light emission which can occur over much longer times after irradiation; it involves storage of energy in metastable states and its release through relatively slow (often thermally activated) processes [14]. Photoluminescence initiated by photo-excitation is the type of luminescence that is discussed in this report.

Luminescence in MOFs generally arises from the building components: conjugated organic linkers and/or metal ions or clusters, although in some cases adsorbed guest molecules may also contribute to the emission [9]. It can occur from direct organic ligands excitation (particularly from the highly conjugated ligands), metal-centered emission (widely observed in rare-earth

MOFs), and charge-transfer such as ligand-to-metal charge transfer (LMCT) and metal-to-ligand charge transfer (MLCT) [13]. (See Figure 1.1b).

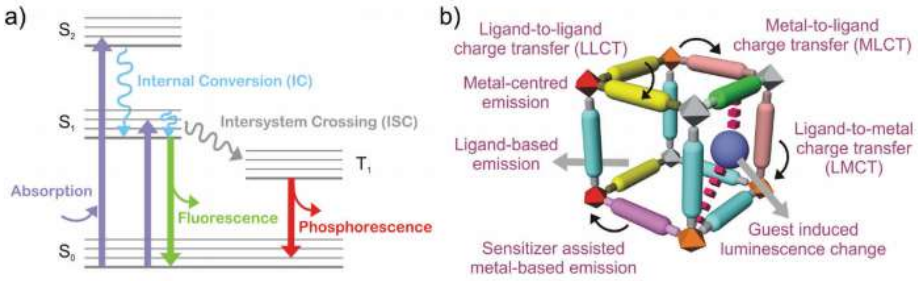

Figure 1.1: *Schematic representation of the various photophysical processes* ***(a)*** *and the different possibilities contributing to the emission of MOFs* ***(b)****, as illustrated by Lustig et al. [7].*

Lanthanide ions are characterized by a gradual filling of the 4f orbitals, from $4f^0$ (for La^{3+}) to $4f^{14}$ (for Lu^{3+}). These electronic $[Xe]4f^n$ configurations (n=0 – 14) generate a variety of electronic energy levels (Figure 1.2). They are well defined due to the shielding of the 4f orbitals by the filled $5s^25p^6$ subshells, and they are less sensitive to the chemical environments around lanthanide ions. Consequently, each lanthanide ion exhibits narrow and characteristic 4f–4f transitions [13].

Rare-earth ions in their trivalent form present prominent transition lines in the visible and near infrared region and, due to the screening of outer electrons, their energy level structure only varies slightly between different host materials [15]. Some of these ions, such as Tb^{3+} and Eu^{3+}, are attractive lumophores [1] because of their spectrally narrow emission, even in solution [17]. The lanthanide ions used to synthesize the LMOFs of interest for this project have been Tb^{3+} and Pr^{3+}, whose energy-level diagrams are shown in Figure 1.3.

[1] Chemical groups that give the property of luminescence to organic compounds [16].

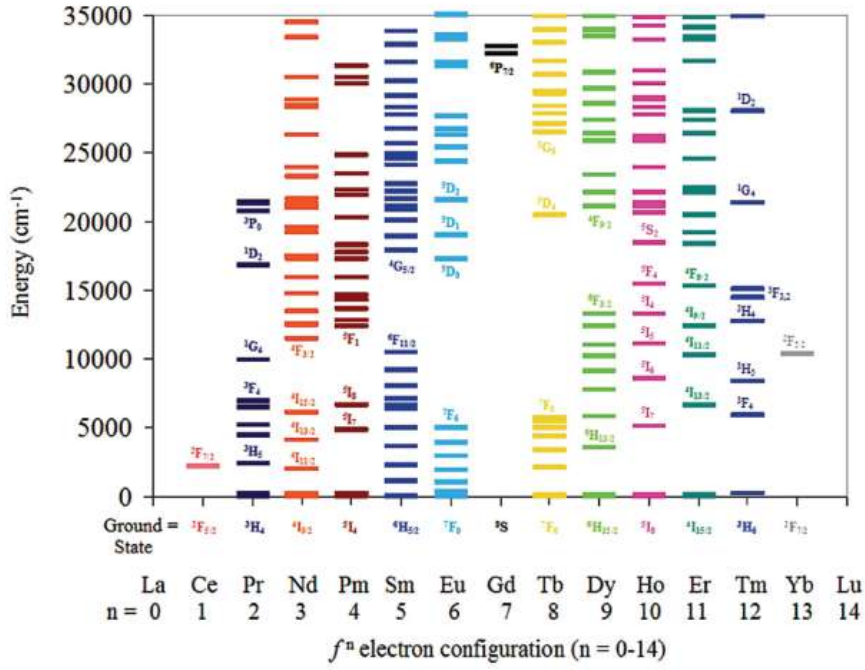

Figure 1.2: *A summary of electronic excited-state energy levels for the Ln(III) series [18] (Copyright 2009 American Chemical Society).*

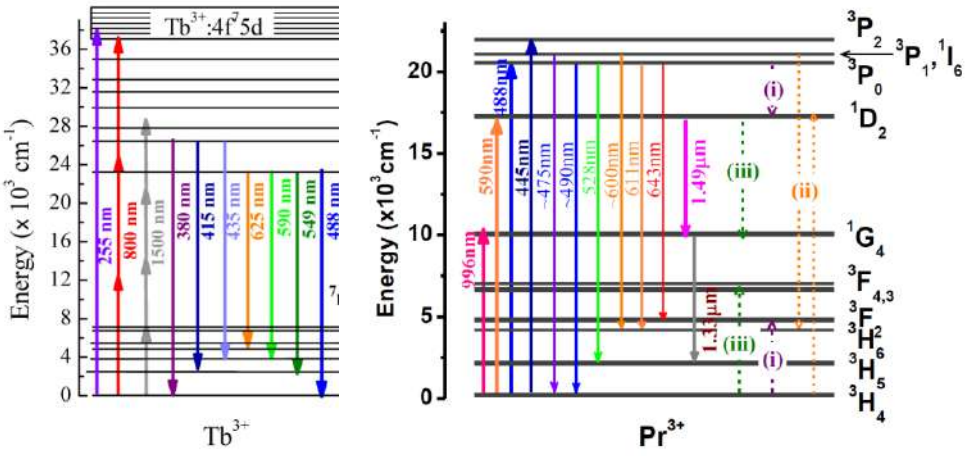

Figure 1.3: *Schematic energy-level diagrams of Tb^{3+} and Pr^{3+} ions and energy transfer processes involved [19, 20].*

1.2.2 Cation Exchange in MOFs

Although the structure and internal environment of the MOFs' pores can be in principle controlled through judicious selection of nodes and organic linkers, the direct synthesis of such materials with desired functionalities in the pores or channels is often difficult to achieve due to their thermal/chemical sensitivity or high reactivity. In this regard, the exchange of free guest molecules or counterions from the cavities, or removal of solvent molecules weakly bound to metal centers constituting frameworks has been frequently exercised [21]. Thus, postsynthetic modification of MOFs –incorporating organic units and metal-organic complexes through reactions with linkers– has emerged as a powerful tool for changing the reactivity of the pores [22].

Chapter 2

Experimental procedure

In this second chapter, the methodology followed in order to synthesize and characterize different luminescent MOFs is described. The synthesis, single-crystal and powder X-ray diffraction and spectroscopic characterization of seven lanthanide coordination polymers constructed from ligand H_4bta are reported.

2.1 Synthesis of the complexes

Reagents and solvents used in all of the syntheses were purchased from commercial sources and used without further purification. The samples were prepared using two different techniques: hydrothermal synthesis (**1** - **3**) and cation exchange (**4** - **7**).

2.1.1 Hydrothermal technique

Compound 1. [Tb(bta)][$(CH_2)_2NH_2$]. A distilled water (5 mL) solution of $Tb(NO_3)_3] \cdot 5H_2O$ (435 mg, 1 mmol) was added dropwise to a dimethylformamide (DMF) solution (5 mL) of 1,2,4,5-benzenetretracarboxylic acid (254 mg, 1 mmol) and stirred 30 min at room temperature. The mixture was sealed in a Teflon-lined stainless steel container, which was heated at

150°C for 3 days. Crystalline powder and some colorless crystals suitable for X-ray diffraction were produced (367 mg), which were filtered off and dried. They exhibit visible green luminescence under UV radiation.

Compound 2. [Pr(bta)][$(CH_2)_2NH_2$]. The preparation method of this complex is similar to that of **1**. An H_2O (5 mL) solution of $Pr(NO_3)_3{\cdot}6H_2O$ (434.91 mg, 1 mmol) was added dropwise to a solution of H_4bta (254 mg, 1 mmol) in 5 mL DMF and stirred 30 min at room temperature. The mixture was sealed in a Teflon-lined stainless steel container, which was heated at 150°C for 3 days. Crystalline powder and some colorless crystals suitable for X-ray diffraction were obtained (406 mg), which were filtered off and dried. They do not exhibit visible luminescence under UV radiation.

Compound 3. $[Tb(bta)]_2$(bpe). A mixture of H_4bta (127 mg, 0.5 mmol) and bpe – 1,2-di(4-pyridyl)ethylene – (91 mg, 0.5 mmol) in 15 mL distilled water was stirred and then a 1 M solution of NaOH (1 mL) was added. A H_2O (15 mL) solution of $Tb(NO_3)_3{\cdot}5H_2O$ (217.5 mg, 0.5 mmol) was added dropwise to the previous solution and stirred 30 min at room temperature. The mixture was sealed in a Teflon-lined stainless steel container, which was heated at 150°C for 3 days. Crystalline powder and some colorless crystals suitable for X-ray diffraction were produced (209 mg), which were filtered off and dried. They exhibit visible green luminescence under UV radiation.

2.1.2 Cation exchange

The general procedure for the cation exchange consists of the suspension of compounds **1** and **2** in a concentrated solution of the desired cation. In this way, the smaller dimethylammonium cation can be exchanged.

Compound 4. [Pr(bta)]$_2$(bpe). An aqueous solution (3 mL H_2O) of bpe (91 mg, 0.5 mmol) was prepared and a solution of HCl was added. This mixture was added dropwise to an aqueous solution (5 mL) where **2** was suspended and stirred 48 h at room temperature. The resulting cation-exchanged sample was filtered off, washed several times with EtOH, and then dried in air. Polycrystalline products were obtained (89 mg). They do not exhibit visible luminescence under UV radiation.

Compound 5. [Tb(bta)](im). A solution of imidazole (34 mg, 0.5 mmol) in 6 mL H_2O and 1 mL of a solution of HCl were added dropwise to a 10 mL H_2O solution of **1** and stirred 72 h at room temperature. The resulting cation-exchanged sample was filtered off, washed several times with H_2O, and then dried in air. Polycrystalline products were obtained (102 mg). They exhibit visible green luminescence under UV radiation.

Compound 6. [Tb(bta)]$_2$(azpy). A solution of azpy – 4,4-azobis(pyridine) – (92 mg, 0.5 mmol) was suspended in 6 mL H_2O and 2 mL HCl 0.5 M was added dropwise to a 10 mL H_2O suspension of **1** and stirred 72 h at room temperature. The resulting cation-exchanged sample was filtered off, washed several times with EtOH, and then dried in air. Polycrystalline products were obtained (72 mg). They exhibit visible green luminescence under UV radiation.

Compound 7. [Tb(bta)](tz). A solution of 1,2,4-triazole (35 mg, 0.5 mmol) in 6 mL H_2O and 1 mL HCl 0.5 M was added dropwise to a 10 mL H_2O suspension of **1** and stirred 72 h at room temperature. The resulting cation-exchanged sample was filtered off, washed several times with H_2O, and dried in air. Polycrystalline products were obtained (68 mg). They exhibit visible green luminescence under UV radiation.

2.2 Characterization

The X-ray diffraction measurements together with the mass spectroscopy and elemental analysis were performed at the *Servicio General de Apoyo a la Investigación* (SEGAI) facilities of the University of La Laguna, in particular at *Servicio Integrado de Difracción de Rayos X* (SIDIX) and *Servicio de Espectrometría de Masas y Análisis Elemental*, respectively. The IR and photoluminescence measurements were carried out at the laboratories of X-Ray and Molecular Materials and Laser Spectroscopy, both belonging to the Physics Department of University of La Laguna.

2.2.1 X-Ray Diffraction

The information relative to the structural arrangement of the atoms in a solid material is an essential requirement in order to understand some physical and chemical properties in detail. Crystals possess a periodic arrangement of their atoms and the structural information about this long-range order can be obtained experimentally by using X-ray diffraction techniques.

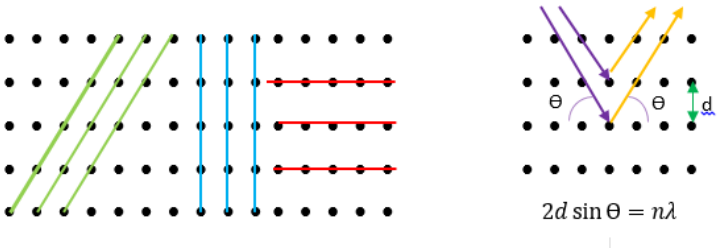

Figure 2.1: *Lattice planes (left) and Bragg's Law (right), the condition for diffraction to occur, where d is the inter-plane distance, n the order of the diffraction peak and θ the scattering angle.*

X-ray diffraction is described as the interference of waves according to the Huygens Fresnel principle and it allows the determination of the atomic and molecular structure of a crystal [23]. When a wavefront of X-rays strikes

an atom, the electrons in that atom interact with the incident radiation and immediately re-emit it. In a crystal, due to the interaction between the X-ray incident beam and the electron density, the beam is diffracted into many specific directions. The diffracted radiation can be collected as well-defined reflections if the sample consists in a single crystal, or as a succession of concentric circles if the sample is polycrystalline.

Single-crystals of **1-3** were mounted on an Agilent SuperNova X-ray diffractometer (Figure 2.2.1) with Cu-Kα radiaton (λ=1.54184 Å) in order to determine the crystal structure of the compounds.

In the case of polycrystalline samples (compounds **4** - **7**), powder X-ray diffraction data were collected in the range $5° < 2\theta < 80°$ on a PANalytical X'pert Pro X-ray diffractometer (Cu-Kα radiaton, λ=1.54184 Å) at room temperature.

Figure 2.2: *SuperNova diffractometer at SEGAI (left) and general view of the X-ray set up (right) with X-ray tube (1), Kappa goniometer (2), X-ray shutter (3), collimator (4), beamstop (5) and Beryllium window (6) [24].*

2.2.2 Elemental Analysis and Mass Spectrometry

Elemental analysis of the samples was performed on a CNHS FLASH EA 1112 analyzer for the simultaneous determination of the percentage of C, N and H. This technique provides the total amount of carbon, nitrogen and hydrogen present in the samples and contributes to the confirmation of the cation exchange.

High resolution mass spectrometry was carried out on a Micromass AutoSpec mass spectrometer in order to obtain information about the composition and structure of the compounds. This technique deals with the analysis of the mass and the fragmentation pattern of the chemical compounds under study.

2.2.3 Spectroscopic Characterization

Infrared spectra

IR spectra (450-4000 cm^{-1}) of complexes **1** - **7** and reactants were recorded on a Shimazdu IRAffinity-1 FTIR (Fourier Transform Infrared) Spectrophotometer.

Absorption spectra

Absorption spectra of **1** - **4** were obtained in the spectral range from 200 to 800 nm by measuring the diffuse reflectance of the polycrystalline samples, at room temperature, using an integrating sphere connected to an Agilent, Cary Series, UV–Vis–NIR Spectrophotometer.

Emission spectra (picosecond pulsed LED)

Based on the results obtained from the absorption measurements, the emission of the compounds **1** - **4** was studied in the range from 400 to 800

nm. The emission spectra of the samples were measured with a fluorescence spectrometer LifeSpec II (Edinburgh Instruments) and the specific software F9000, using a picosecond pulsed light emitting diode EPLED-375 nm (dwell time: 1 s; step: 1nm).

Emission and excitation spectra (Xe lamp)

Excitation and emission spectra of the prepared MOFs (**1** - **7**) were also obtained by using a xenon lamp as source of excitation. The calibration curve of the excitation lamp was measured and taken into account in all the emission measurements.

Excitation spectra of the Tb-complexes were measured in the range from 210 to 525 nm (step: 1 nm; time: 1000 ms) detecting in 545 nm (transition $^5D_4 \rightarrow {}^7F_5$ of the Tb^{3+} ion), with an attenuator of optical density (OD) 0.6 and an LP530 filter. In order to get the emission spectra, the samples were excited at 320 nm and scans were carried out from 400 to 750 nm (step: 1 nm; time: 1000 ms); measurements were performed using the same attenuator of OD 0.6 and an LP395 filter. In the case of the Pr-complexes, two filters were used (LP550 and LP530) and samples were excited at 445 nm to get the emission spectra, while the excitation spectra were achieved at 620 nm (detection wavelength corresponding to the energetic transition $^3P_0 \rightarrow {}^3H_6$ of the Pr^{3+} ion) and using an LP550 filter.

Luminescence decay

Photoluminescence lifetime measurements were performed in a fluorescence spectrometer LifeSpec II by Edinburgh Instruments using the specific software F9000. Samples of the complexes **1** - **4** were excited by a picosecond pulsed light emitting diode EPLED-375 nm and scans were carried out from 400 to 800 nm with dwell time of 1 s and step of 1 nm.

Chapter 3

Results and Discussion

The results obtained from the experimental procedure previously described are presented and analyzed. This chapter focuses on the exposition and description of the crystal structures solved, as well as on the study of the outcomes concerning to the cation exchange and the spectroscopic characterization.

3.1 Description of the structures

The structures of compounds **1** - **3** were solved and refined using the SHELXS program [25] included in the OLEX2 software package [26] and the final geometrical calculations and graphical manipulations were carried out with Diamond 4 [27]. The powder diffraction patterns analysis of the polycrystalline samples was performed with FullProf Suite [28].

Compound 1. [Tb(bta)][$(CH_2)_2NH_2$]·H_2O. (H_4bta is the 1,2,4,5-benzenetetracarboxylic acid and $(CH_2)_2NH_2$ is the dimethylammonium ca-tion). The crystal structure of **1** consists of an anionic three-dimensional network with pores where the dimethylammonium cations and the water molecules are located. The anionic 3D network is formed by oxo-bridged chains of

Tb(III) ions which run along the crystallographic a axis linked to four adjacent ones through the bta ligands. This anionic framework creates somewhat rectangular pores of approx. 11 x 9 $Å^2$ extended also in the a direction. The Tb(III) ion is eight-coordinate in a distorted square antiprism environment, whereas the bta ligand is able to coordinate to six Tb(III) ions of two different oxo-bridged terbium chains.

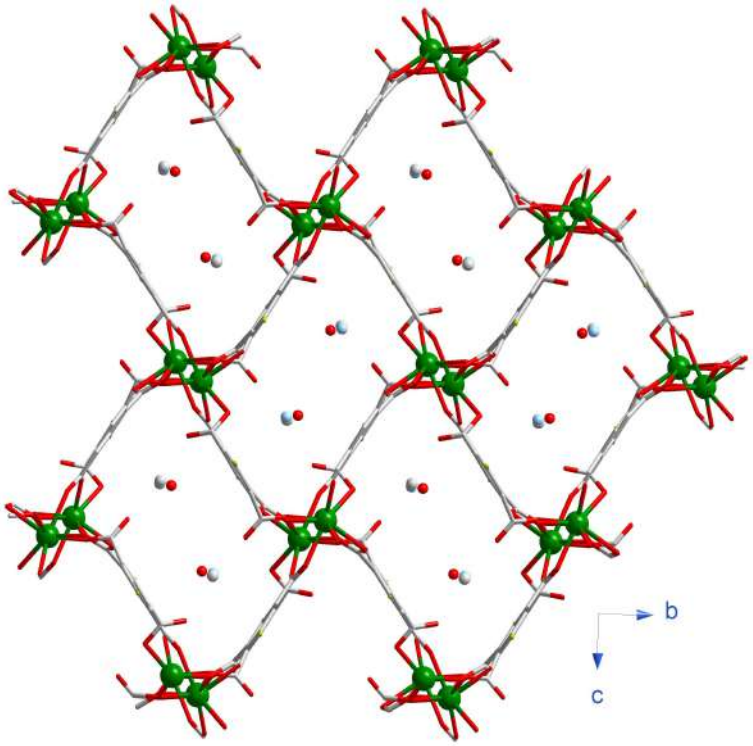

Figure 3.1: *Projection view along the a axis of compound **1**.*

Compound 2. $[Pr(bta)][(CH_2)_2NH_2]\cdot 3H_2O$. ($H_4$bta is the 1,2,4,5-benzenetetracarboxylic acid and $(CH_2)_2NH_2$ is the dimethylammonium cation). The crystal structure of **2** is quite similar to that of 1. A 3D anionic network is formed where the oxo-bridged Pr(III) chains running along the a axis are linked by the bta ligands. The pores have a diamond-like shape with dimensions approx. 11 x 9 $Å^2$ extended in the a direction. The Pr(III) ion is nine-coordinated in 2 to form a tricapped trigonal prism polyhedron. There

are two crystallographically independent bta ligands in 2, both of them able to coordinate six Pr(III) cations. The dimethylammonium cations located in the pores establish hydrogen bonds N–H···O with the uncoordinated carboxylate oxygen atoms of the anionic framework.

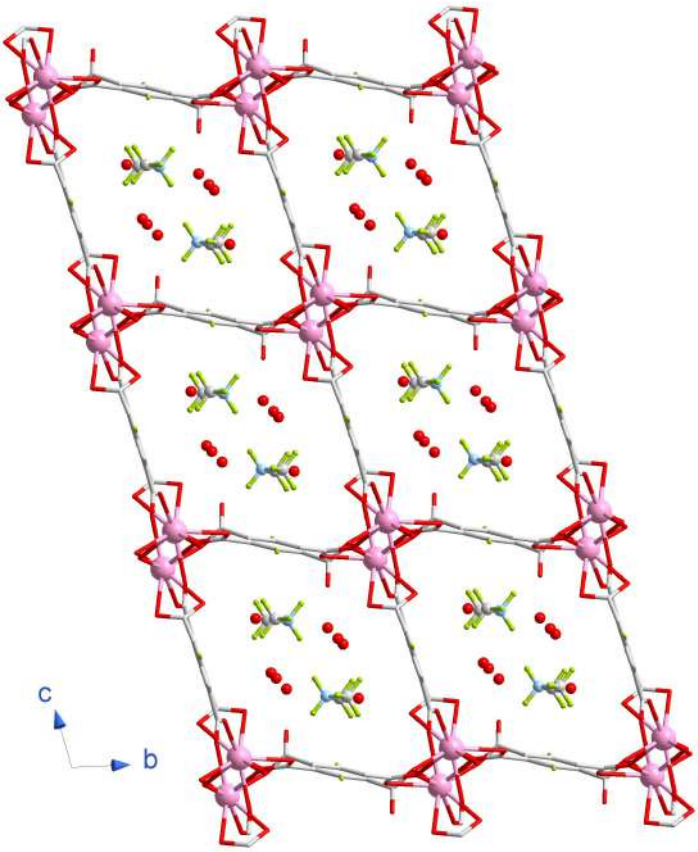

Figure 3.2: *Projection view along the a axis of compound* ***2****.*

Compound 3. [Tb(bta)]$_2$(H$_2$bpe). (H_4bta is the 1,2,4,5-benzenetetracarboxylic acid and bpe is the 1,2-bis(4-pyridyl)ethylene). The crystal structure of **3** is similar to that of **1** and **2**. The three-dimensional anionic framework is formed by oxo-bridged terbium(III) chains running along the a axis which are linked by the bta ligands. The pores are now almost square-shaped with approximate dimensions of 11 x 10 Å^2. The H_2bpe cations are located in

these pores leaving no room to accommodate further water molecules as occur in **1** and **2**, but they establish N–H···O hydrogen bonds in a similar way as the dimethylammonium cations do in **2**. The unique crystallographic Tb(III) ion in **3** is eight-coordinate with a square antiprism environment. There are two crystallographically independent bta ligands (as occurs in **2**) which coordinate to six Tb(III) ions.

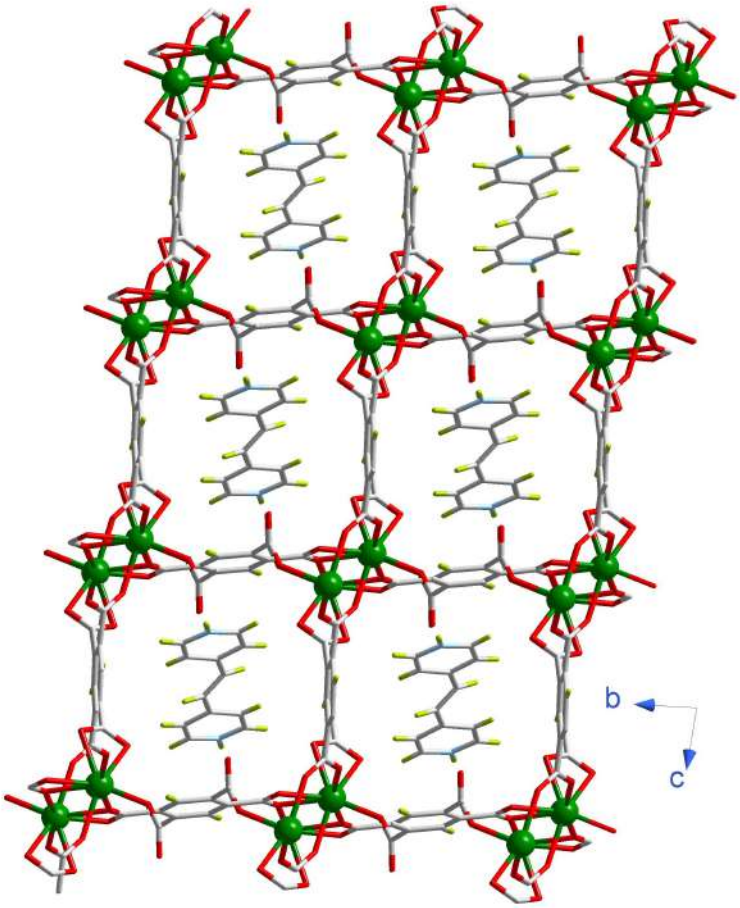

Figure 3.3: *Projection view along the a axis of compound **3**.*

Powder X-ray diffraction analysis performed on the polycrystalline samples reveals that Pr-complexes (**2** and **4**) share the same crystal structure (see powder XRD patterns in Figure 3.4). Despite the inclusion of the new

guest in **4**, the 3D net remains unchanged. However, as illustrated in Figure 3.5, each Tb-complex has a different crystal structure, which is known for compounds **1** and **3** thanks to single-crystal X-ray diffraction but cannot be deduced for polycrystalline compounds **5** - **7**, unless suitable X-ray diffraction crystals were grown.

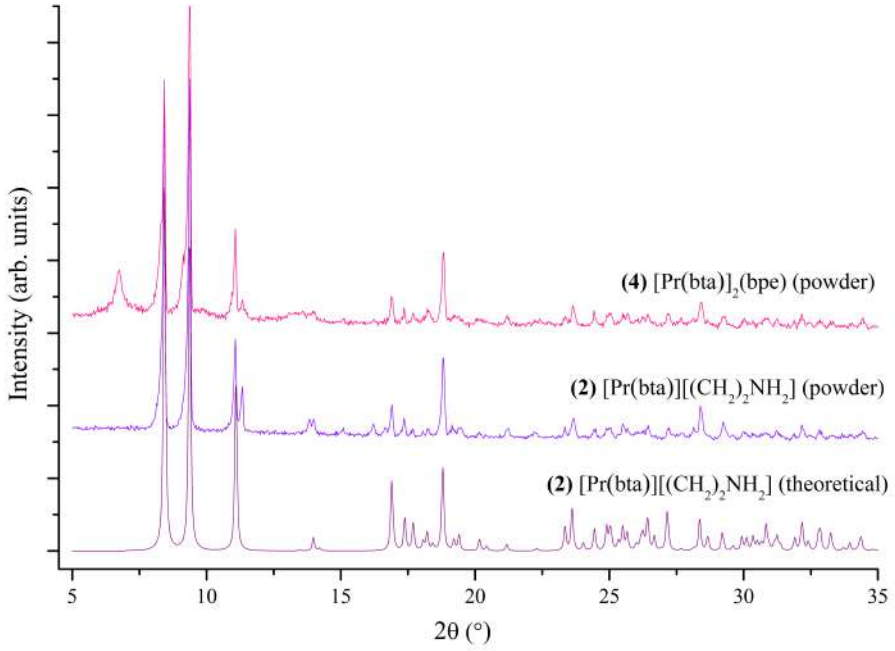

Figure 3.4: *Powder X-ray diffraction analysis of Pr-compounds. Theoretical (obtained from the SCXRD data) and powder patterns of* ***2*** *and powder XRD pattern of* ***4****.*

3.2 Cation exchange

The results collected from mass spectrometry and elemental analysis support the evidence of the cation exchange, as well as those provided by powder X-ray diffraction. Variations on the powder XRD patterns of the compounds demonstrate that the reaction has taken place, the structures have changed and, thus, different MOFs have been obtained.

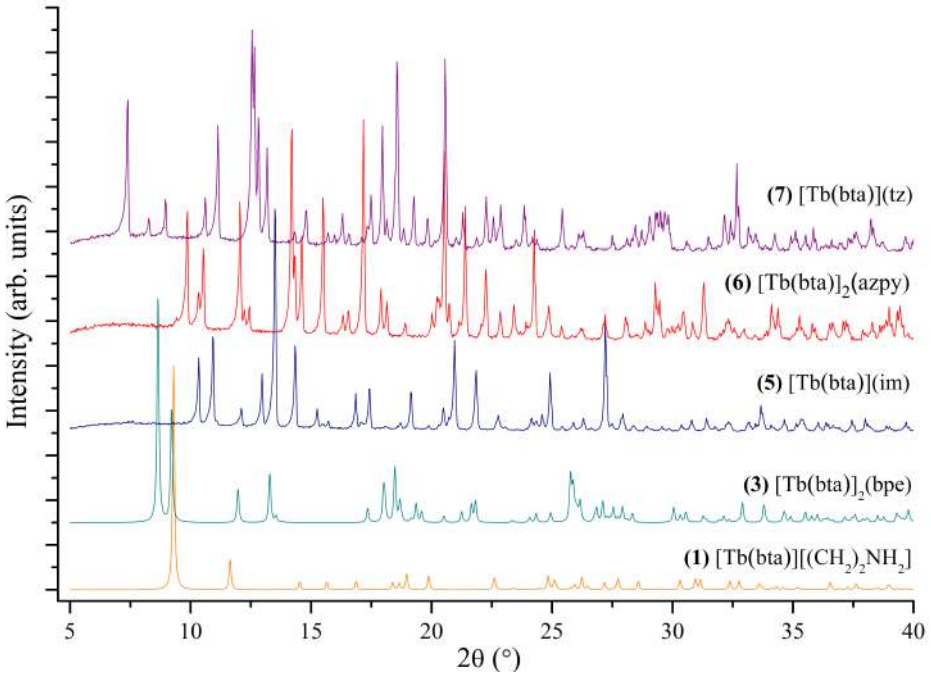

Figure 3.5: *Powder X-ray diffraction analysis of Tb-compounds. Theoretical (obtained from the SCXRD data) powder XRD patterns of **1** and **3**, and experimental PXRD patterns of **5** - **7**.*

Mass spectrometry and elemental analysis show the presence of bpe in complex **4** $[Pr(bta)]_2(bpe)$, which indicates that the dimethylammonium molecules of complex **3** $[Pr(bta)][(CH_2)_2NH_2]$ have been successfully exchanged for the bpe. In particular, **3** is found to be tetra-hydrated, with approximately 28.39% C, 2.45% N and 2.30% H, while **3** is hexa-hydrated, with 31.48% C, 2.93% N and 2.48% H, which agrees with the values expected. Mass spectrometry and elemental analysis of the rest of the complexes are waiting to be performed.

3.3 Spectroscopic results

Lastly, the results of the spectroscopic measurements previously performed are interpreted. The data analysis has been carried out using Orig-

inPro 8 software [29].

Infrared spectra

IR spectra of the Pr- (**2** and **4**) and Tb-complexes (**1**, **3**, **5**, **6** and **7**), as well as of the reactants employed in the syntheses (H_4bta, bpe, azpy, 1,2,4-triazole and imidazole), were measured in the range from 350 to 4000 cm^{-1}.

The infrared spectra of Figure 3.6 show that compound **3** contains bpe and is similar to **1**, since it presents peaks in common with the other two spectra.

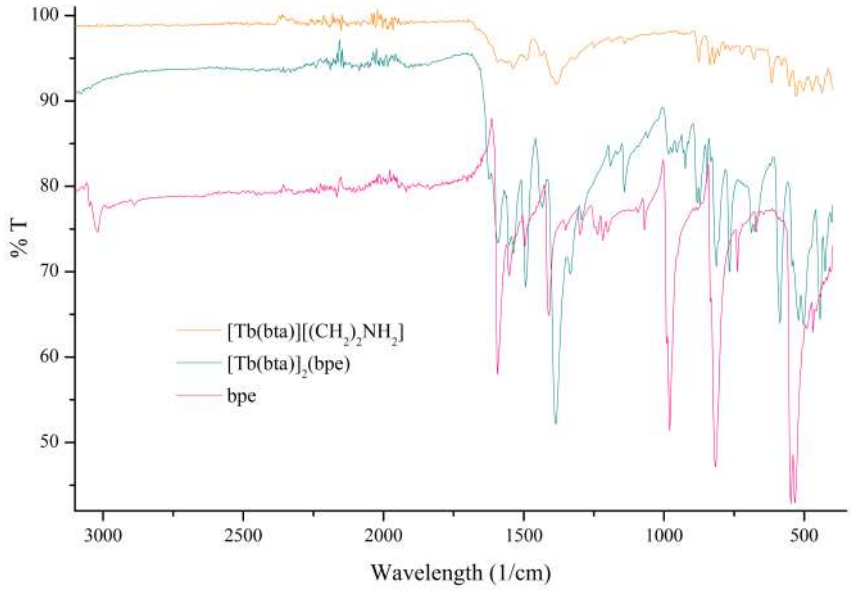

Figure 3.6: *IR spectra of complexes **1** (orange) and **3** (blue) and bpe (pink).*

Cation exchange is confirmed by IR characterization, as can be checked in Figures 3.7 - 3.10: the cation exchanged complexes show IR peaks also present in the initial compound and the corresponding cation.

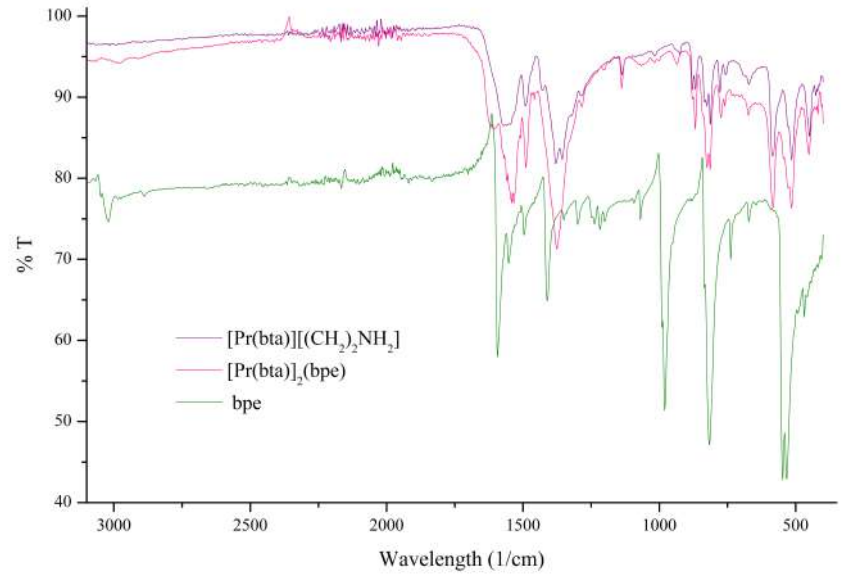

Figure 3.7: *IR spectra of complexes* ***2*** *(purple) and* ***4*** *(pink) and bpe (green).*

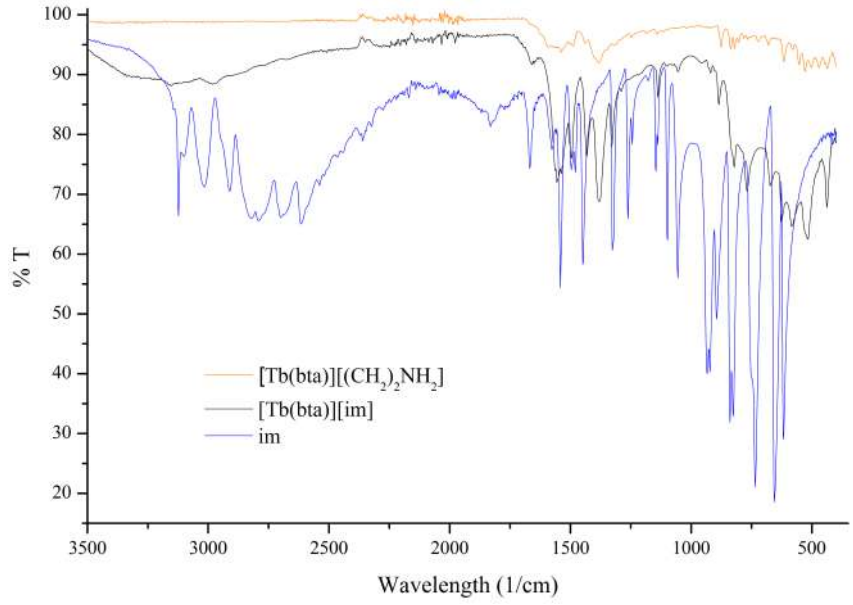

Figure 3.8: *IR spectra of complexes* ***1*** *(orange) and* ***5*** *(black) and imidazole (blue).*

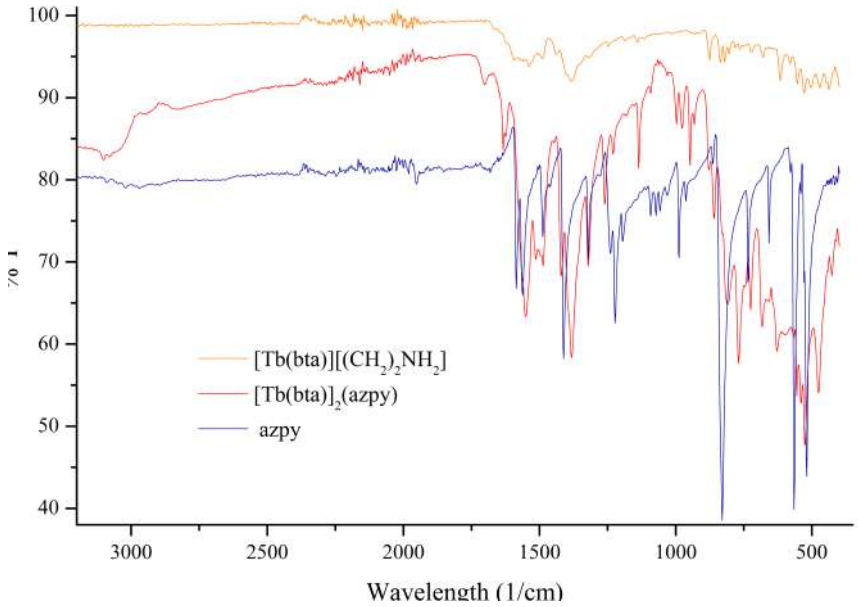

Figure 3.9: *IR spectra of complexes* ***1*** *(orange) and* ***6*** *(red) and azpy (blue).*

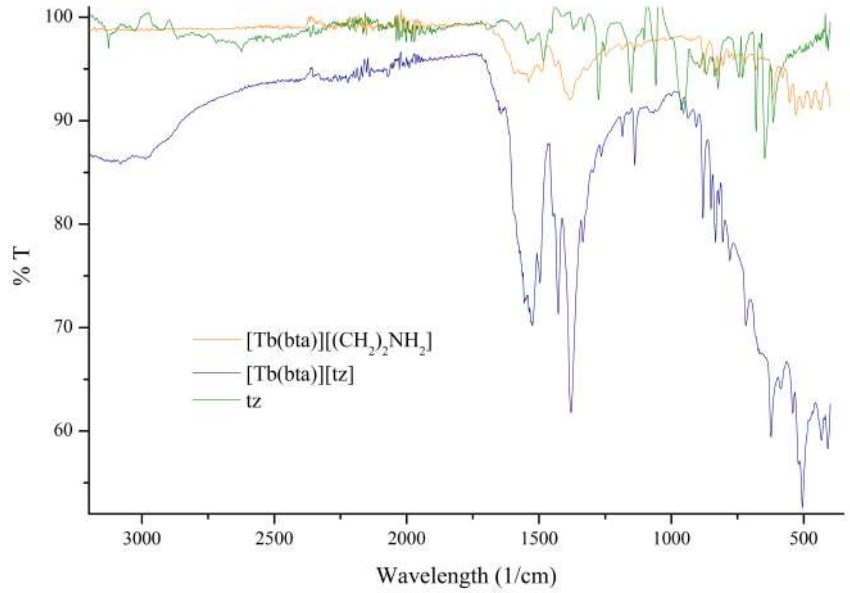

Figure 3.10: *IR spectra of complexes* ***1*** *(orange) and* ***7*** *(blue) and 1,2,4-triazole (green).*

Absorption spectra

The absorption spectra from 200 to 800 nm obtained for the Tb^{3+}-complexes **1** and **3**, the two Pr^{3+}-complexes (**2**, **4**) and some of the reactants employed to synthesize them (H_4bta, bpe, dimethylammonium chloride and $T(bNO_3)_3{\cdot}5H_2O$) are shown in Figure 3.11.

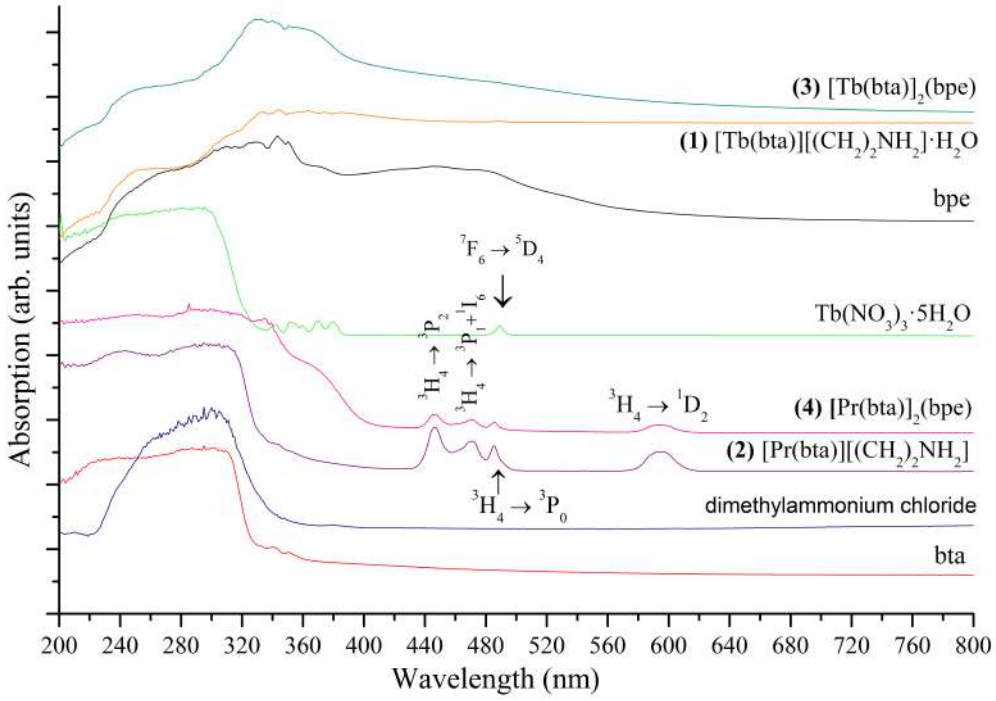

Figure 3.11: *Normalized absorption spectra of compounds **1** - **4** and reactants. The transitions from the ground state ($^7F_6$ for Tb^{3+} ion, $^3H_4$ for Pr^{3+} ion) to the corresponding excited states are labeled.*

A broad absorption band can be observed in the UV range of the electromagnetic spectra (from 200 to approximately 330 nm), which corresponds to the absorption of the ligand (H_4bta). Some well-defined absorption peaks appear from around 420 nm to 640 nm. These peaks correspond to the following energetic transitions: in the case of the Tb^{3+}-complexes, the transition from the ground state $^7F_6$ to the excited state $^5D_4$ at around 488 nm

can be distinguished (more clearly seen in $Tb(NO_3)_3$); while for the Pr^{3+}-complexes we can find transitions from the ground state $^3H_4$ to the excited states $^3P_2$ at 445 nm, $^3P_1$+$^1I_6$ at 475 nm, $^3P_0$ at 490 nm and $^1D_2$ at 600 nm. The presence of bpe (1,2-di(4-pyridyl)ethylene) can also be recognized in complexes **3** and **4**, decreasing the intensity of the transitions with respect to those not containing this compound.

Emission spectra (picosecond pulsed LED)

Emission spectra of complexes **1** - **4** were obtained under excitation of the samples with a 375 nm wavelength. The characteristic emission bands of Tb^{3+} (see Figure 1.3) were observed at 490 nm ($^5D_4 \rightarrow {}^7F_6$), 546 nm ($^5D_4 \rightarrow {}^7F_5$), 586 nm ($^5D_4 \rightarrow {}^7F_4$) and 623 nm ($^5D_4 \rightarrow {}^7F_{2,3}$) and are labeled in Figure 3.12.

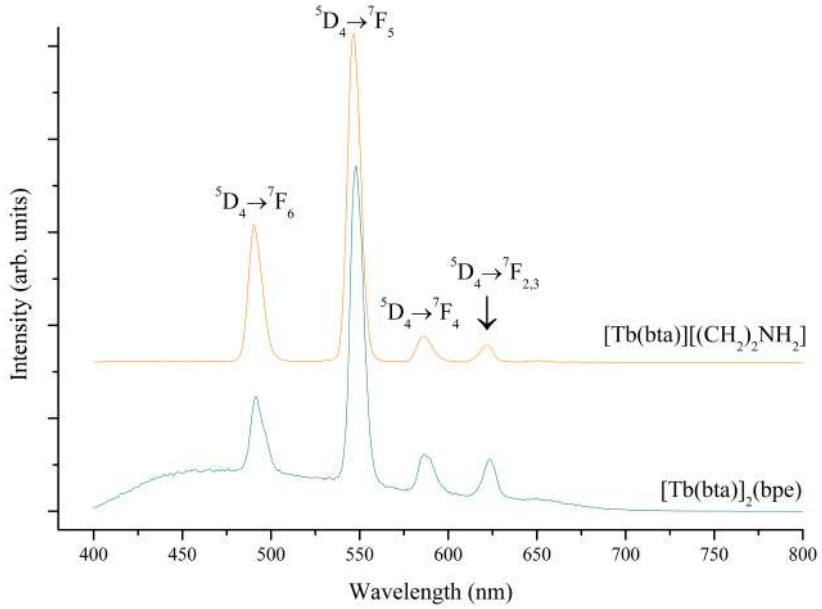

Figure 3.12: *Emission spectra of Tb^{3+}-complexes **1** (orange) and **3** (blue) under excitation at 375 nm. The energetic transitions corresponding to the main energy levels of Tb^{3+} ion are labeled.*

The strongest Tb^{3+} emission comes from the $^5D_4 \rightarrow {}^7F_5$ and $^5D_4 \rightarrow {}^7F_6$ transitions, giving rise to the strong green luminescence (495 - 570 nm) characteristic of Tb^{3+} complexes. Moreover, the presence of bpe in the structure influences the emission of the complex **3**, since bpe also presents green luminescence when excited with UV radiation. For the Pr^{3+} complexes, the characteristic emission band (see Figure 3.13) appears at about 621 nm ($^3P_0 \rightarrow {}^3H_6$), which explains the red emission observed in the samples when they were excited with 375 nm radiation.

By comparing the emission spectra of the Pr^{3+} complexes with the absorption ones in the range from 400 to 610 nm, the presence of the energetic transitions $^3H_4 \rightarrow {}^3P_2$, $^3H_4 \rightarrow {}^3P_1{+}^1I_6$, $^3H_4 \rightarrow {}^3P_0$ and $^3H_4 \rightarrow {}^1D_2$ can be observed as reabsorption of the ligand luminescence due to energy transfer from the ligand to the metal center. Absorption spectrum has been added to the figure to show that the reabsorption corresponds to the overlap between the ligand emission band and the Pr3+ ground state absorption.

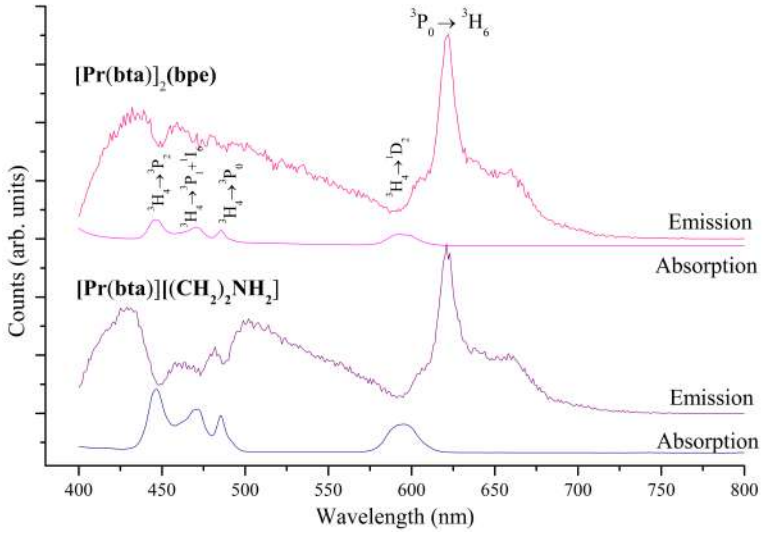

Figure 3.13: *Emission and absorption spectra of Pr^{3+}-complexes **2** (botom) and **4** (top) plotted together for comparison issues.*

Emission and excitation spectra (Xe lamp)

Excitation spectra of the Tb complexes are illustrated in Figure 3.14, detecting at 545 nm and scanning from 210 to 525 nm. The excitation spectra of these compounds present broad bands arising from ligand-to-metal energy transfer and narrow bands from RE (rare-earth) 4f-intraconfigurational transitions.

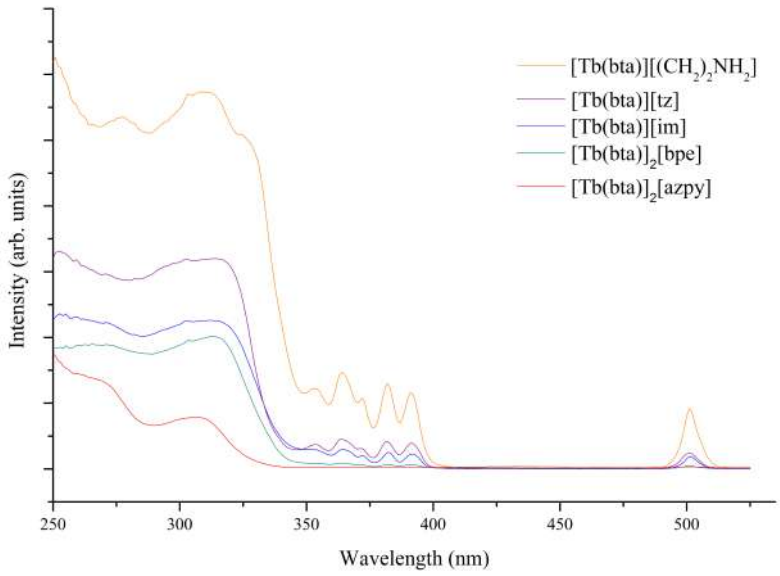

Figure 3.14: *Excitation spectra of Tb-complexes. The spectrum of Tb(H_4bta) [azpy] (**6**) is amplified by a factor 400.*

Emission spectra of the terbium-based MOFs were obtained under excitation of the samples with a 320 nm wavelength (Figure 3.15). The characteristic emission bands of the isolated Tb^{3+} ion can be observed at 492 nm ($^5D_4 \rightarrow {}^7F_6$), 547 nm ($^5D_4 \rightarrow {}^7F_5$), 587 nm ($^5D_4 \rightarrow {}^7F_4$) and 621 nm ($^5D_4 \rightarrow {}^7F_{2,3}$). The most significant transition is $^5D_4 \rightarrow {}^7F_5$ at λ=547 nm, which is responsible for the strong green luminescence characteristic of this ion.

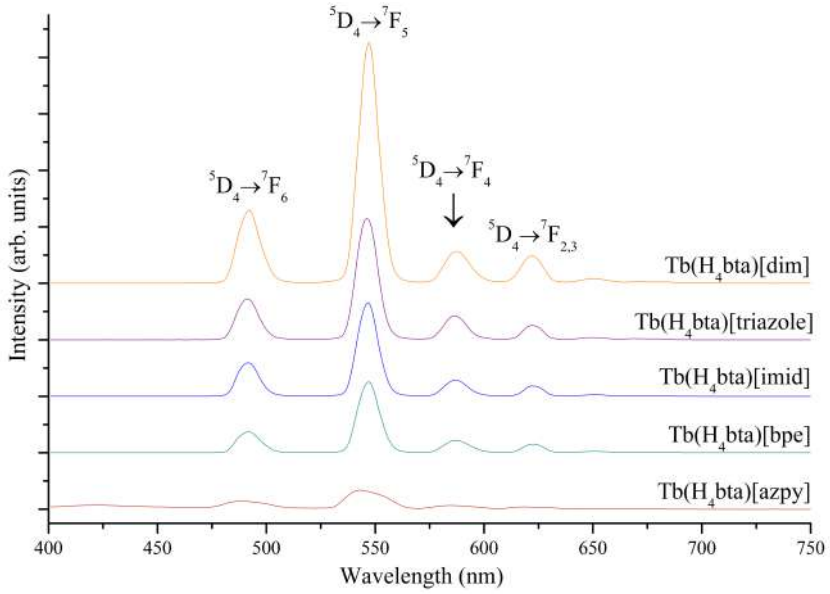

Figure 3.15: *Emission spectra of Tb^{3+}-complexes under excitation at 320 nm. The spectrum of [Tb(bta)]$_2$(azpy) (**6**) is amplified by a factor 400. All spectra have been corrected from the Xe lamp spectral response.*

As previously concluded, there exists photon transfer from the ligand to the metal in the Pr^{3+} complexes in the range from 400 to 610 nm (Figure 3.16). The characteristic Pr ion emission band (see Figure 3.17) appears at about 619 nm ($^3P_0 \rightarrow {}^3H_6$), and another band is detected at 568 nm. The weak emission spectrum of Figure 3.17 corresponds to the tail of the ligand emission band. Note that the emission decrease at about 600 nm is due to energy transfer from the ligand to the Pr metal center, which shows an absorption band at 600 nm. This confirms that there exists energy interaction between the ligand and the metal moieties in the MOFs.

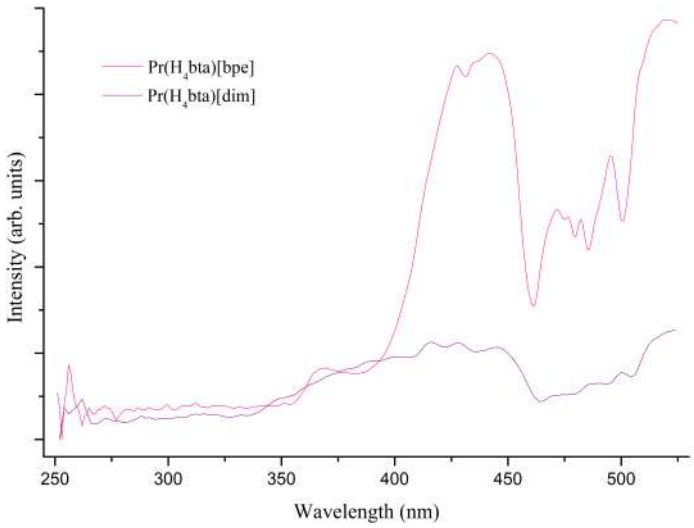

Figure 3.16: *Excitation spectra of Pr^{3+}-complexes.*

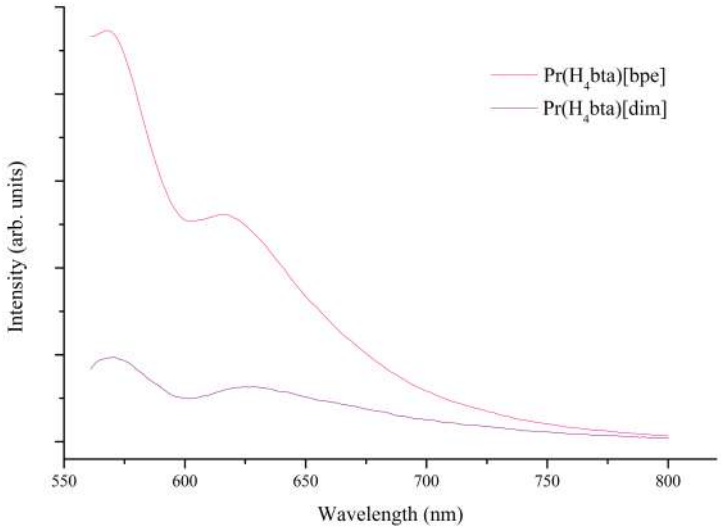

Figure 3.17: *Emission spectra of Pr^{3+}-complexes under excitation at 445 nm. All spectra have been corrected from the Xe lamp spectral response.*

In order to compare the emission intensity of the green luminescent MOFs (the Tb-based ones), in the following bar graph (Figure 3.18) a comparison of the integrated intensities from the emission curves (Figure 3.15) of each terbium sample is presented. From higher to lower emission, the compounds are: [Tb(bta)][$(CH_2)_2NH_2$] (**1**), [Tb(bta)][tz] (**7**), [Tb(bta)][im] (**5**), $[Tb(bta)]_2$[bpe] (**3**) and $[Tb(bta)]_2$[azpy] (**6**).

Compound	**Intensity (arb. units)**
[Tb(bta)][$(CH_2)_2NH_2$] (**1**)	167.16
$[Tb(bta)]_2$[bpe] (**3**)	52.73
[Tb(bta)][im] (**5**)	67.89
$[Tb(bta)]_2$[azpy] (**6**)	0.0876
[Tb(bta)][tz] (**7**)	90.32

Table 3.1: Integrated intensities of the Tb-based MOFs.

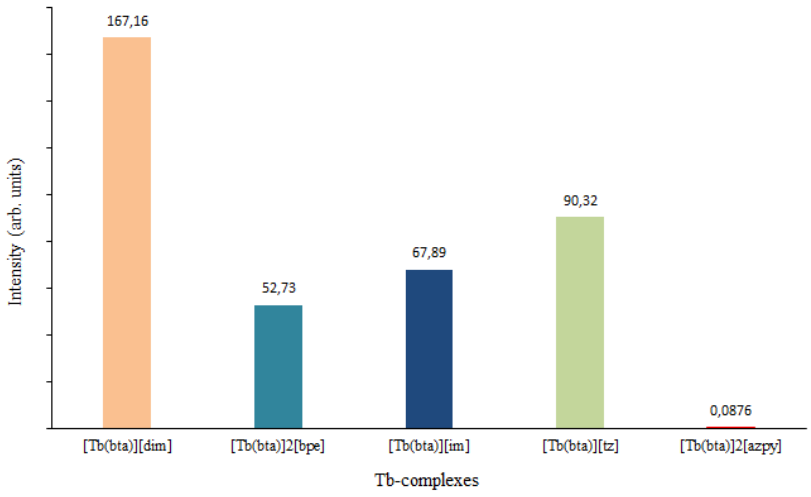

Figure 3.18: *Bar diagram showing the total intensity emitted by each one of the terbium-complexes. These intensities have been calculated from the integration of the emission spectra.*

Luminescent decay

Samples of **1** - **4** were excited at 370 nm. The emission of [Tb(bta)] $[(CH_2)_2NH_2]$ (**1**) and $[Tb(bta)]_2$[bpe] (**3**) was measured in 450 nm, while it was detected in 430 nm for [Pr(bta)]$[(CH_2)_2NH_2]$ (**2**) and $[Pr(bta)]_2$[bpe] (**4**). The resulting curves showing the emission intensity versus the time in nanoseconds are presented in Figure 3.19. It shows quite short lifetimes of the complexes, meaning that there exists ligand-to-metal photon transfer, and besides the decay rate is faster for the Pr-based MOFs than for the Tb-based ones.

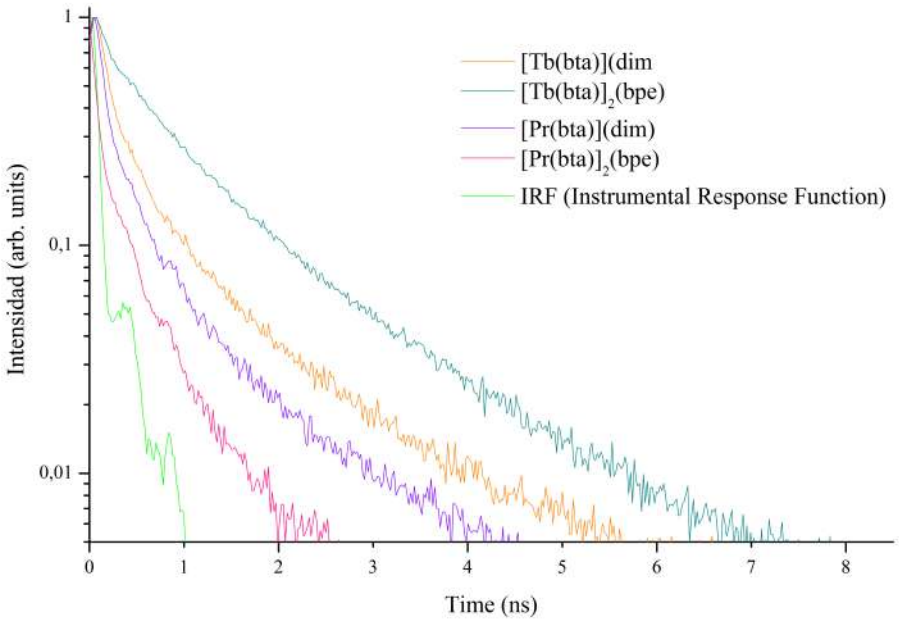

Figure 3.19: *Photoluminescence intensity in 450 nm (Tb-complexes) and 430 nm (Pr-complexes) versus time (ns). Intensity is presented normalized and in logarithmic scale.*

The non-exponential character of the decay is characteristic of solid powder samples. In order to quantify the average lifetime value of the fluorescence, the decay curves have been successfully fitted to a double exponential decay of the type:

$$I(t) = A_1 e^{-t/\tau_1} + A_2 e^{-t/\tau_2} \tag{3.1}$$

For each sample, the resulting parameters are:

Compound	**Coefficient**	**Value (ns)**	**Standard error**
1	τ_1	1.552	0.129
1	τ_2	0.262	0.007
3	τ_1	0.506	0.021
3	τ_2	1.544	0.078
2	τ_1	0.196	0.005
2	τ_2	1.266	0.124
4	τ_1	0.072	$6.3{\cdot}10^{-4}$
4	τ_2	0.515	0.007

Table 3.2: Parameters of the double exponential fitting.

In Table 3.2 we can see that there is a longer and a shorter lifetime for each sample. The average lifetime is calculated from this fitting by using the expression:

$$< \tau >= \frac{A_1\tau_1^2 + A_2\tau_2^2}{A_1\tau_1 + A_2\tau_1} \tag{3.2}$$

The resulting average lifetime values of the fluorescence for each samples are summarized in Table 3.3.

Compound	**Lifetime (ns)**
[Tb(bta)][$(CH_2)_2NH_2$] (**1**)	0.856
[Tb(bta)]$_2$[bpe] (**3**)	1.376
[Pr(bta)][$(CH_2)_2NH_2$] (**2**)	0.644
[Pr(bta)]$_2$[bpe] (**4**)	0.367

Table 3.3: Average lifetime value of the fluorescence for compounds **1** - **4**.

Chapter 4

Conclusions and future work

This final chapter includes an overview of the results achieved. To conclude, some future prospects are suggested.

4.1 Conclusions

Seven new lanthanide metal-organic frameworks have been synthesized and characterized, and their luminescent properties have been described. The efficient inclusion of selected molecules in the pores of these MOFs via cation exchange has been demonstrated.

The crystal structures of complexes **1** - **3** are quite similar, consisting of a 3D anionic networks where the oxo-bridged Ln(III) chains running along the a axis are linked by the bta ligands. Despite powder X-ray diffraction analysis of **4** reveals that it has the same structure as **2**, the crystal structures of the terbium-compounds resulting from the cation exchange are not similar with that of the starting complex (**1**). However, evidence of the photon transfer from the ligand to the metal is provided by emission and excitation spectra. These Ln-based MOFs exhibit their characteristic luminescence at an excitation of 320 nm (Tb) and 445 nm (Pr).

The Tb-based MOFs emit visible green luminescence under UV radiation. The emission bands centered in 492 nm, 547 nm, 587 nm and 621 nm obtained under 320 nm excitation were identified as the following transitions of the Tb^{3+} ion: $^5D_4 \rightarrow {}^7F_6$, $^5D_4 \rightarrow {}^7F_5$, $^5D_4 \rightarrow {}^7F_4$ and $^5D_4 \rightarrow {}^7F_{2,3}$, respectively. Despite the Pr-based MOFs mostly emit in the IR spectral range, the transition $^3P_0 \rightarrow {}^3H_6$ at about 620 nm has been detected under 375 nm excitation. The average lifetimes of the fluorescence of MOFs **1** - **4** under 375 nm excitation are obtained by fitting the luminescence decay curves measured for each sample.

4.2 Future of the project

Some future prospects can be summarized in the following issues:

1. Due to their luminescent properties, the dispersion of these new MOFs in a polymer matrix could be an interesting experiment to perform in order to utilize them in solar cells.

2. The optical properties of LMOFs are often affected by temperature. For example, fluorescence intensity typically decreases as the temperature increases [9]. In this regard, temperature-dependent analyses of the complexes prepared would be of great significance.

3. It could be interesting to perform a study of the variable temperature PXRD patterns and thermogravimetric experiments in order to reveal if compounds are (highly) thermal stable, which is an important parameter for potential practical use of porous MOFs in gas/vapor separation applications.

4. In metal-organic frameworks containing either 1,2,4-triazole or imidazole in their pores, electroluminescence becomes a very interesting

phenomenon to study. Due to their structure and their way to order inside the pores of the MOFs, these organic compounds could conduct electricity and the MOFs could emit light in response to the passage of an electric current or to a strong electric field.

Chapter 5

Acknowledgements

I would first like to thank my thesis advisor Dr. Jorge Pasán García of the X-ray and Molecular Materials Laboratory at University of La Laguna. His guidance helped me in all the time of research and writing of this thesis. I would also like to thank Dra. Catalina Ruiz and my fellow labmates Ana, Carla, Ariel, Mariadel and Paola, who helped me several times when I run into a trouble spot.

I would also like to thank Prof. Fernando Lahoz of Laser Spectroscopy Laboratory at University of La Laguna with whom I carried out the luminescence measures and who helped me to understand and perform the calculations involved in this project.

Finally, I must express my very profound gratitude to my parents for providing me with unfailing support and continuous encouragement. This accomplishment would not have been possible without them. Thank you.

References

[1] S. Yuan, L. Feng, K. Wang, J. Pang, M. Bosch, C. Lollar, Y. Sun, J. Qin, X. Yang, P. Zhang, *et al.*, "Stable metal–organic frameworks: Design, synthesis, and applications," *Advanced Materials*, p. 1704303, 2018.

[2] L. Cañadillas-Delgado, J. Pasán, O. Fabelo, M. Hernández-Molina, F. Lloret, M. Julve, and C. Ruiz-Pérez, "Two-and three-dimensional networks of gadolinium (iii) with dicarboxylate ligands: synthesis, crystal structure, and magnetic properties," *Inorganic chemistry*, vol. 45, no. 26, pp. 10585–10594, 2006.

[3] B. Gil-Hernández, J. K. Maclaren, H. A. Höppe, J. Pasan, J. Sanchiz, and C. Janiak, "Homochiral lanthanoid (iii) mesoxalate metal–organic frameworks: synthesis, crystal growth, chirality, magnetic and luminescent properties," *CrystEngComm*, vol. 14, no. 8, pp. 2635–2644, 2012.

[4] H. Furukawa, K. E. Cordova, M. O'Keeffe, and O. M. Yaghi, "The chemistry and applications of metal-organic frameworks," *Science*, vol. 341, no. 6149, p. 1230444, 2013.

[5] S. R. Batten, N. R. Champness, X.-M. Chen, J. Garcia-Martinez, S. Kitagawa, L. Öhrström, M. O'Keeffe, M. P. Suh, and J. Reedijk, "Coordination polymers, metal–organic frameworks and the need for terminology guidelines," *CrystEngComm*, vol. 14, no. 9, pp. 3001–3004, 2012.

[6] O. M. Yaghi, M. O'Keeffe, N. W. Ockwig, H. K. Chae, M. Eddaoudi, and J. Kim, "Reticular synthesis and the design of new materials," *Nature*, vol. 423, no. 6941, p. 705, 2003.

[7] W. P. Lustig, S. Mukherjee, N. D. Rudd, A. V. Desai, J. Li, and S. K. Ghosh, "Metal–organic frameworks: functional luminescent and photonic materials for sensing applications," *Chemical Society Reviews*, vol. 46, no. 11, pp. 3242–3285, 2017.

[8] L. Canadillas-Delgado, O. Fabelo, J. Pasán, M. Déniz, C. Martínez-Benito, P. Díaz-Gallifa, T. Martín, and C. Ruiz-Pérez, "Three new europium (iii) methanetriacetate metal-organic frameworks: the influence of synthesis on the product topology," *Acta Crystallographica Section B: Structural Science, Crystal Engineering and Materials*, vol. 70, no. 1, pp. 19–27, 2014.

[9] Z. Hu, B. J. Deibert, and J. Li, "Luminescent metal–organic frameworks for chemical sensing and explosive detection," *Chemical Society Reviews*, vol. 43, no. 16, pp. 5815–5840, 2014.

[10] S. Dao-Feng, B. Wen-Hua, C. Rong, L. Xing, S. Qian, and H. Mao-Chun, "Hydrothermal synthesis and structure of a new 3d lanthanide-carboxylate framework,[la (btec) 1/2 (h2btec) 1/2 (h2o)] n (h4btec= 1, 2, 4, 5-benzenetetracarboxylic acid)," *Chinese Journal of Chemistry*, vol. 21, no. 4, pp. 405–408, 2003.

[11] O. Fabelo, J. Pasán, L. Cañadillas Delgado, F. S. Delgado, A. Labrador, F. Lloret, M. Julve, and C. Ruiz-Pérez, "(4,4) rectangular lattices of cobalt(ii) with 1,2,4,5-benzenetetracarboxylic acid: influence of the packing in the crystal structure," *Crystal Growth and Design*, vol. 8, no. 11, pp. 3984–3992, 2008.

[12] J. Ferrando-Soria, H. Khajavi, P. Serra-Crespo, J. Gascon, F. Kapteijn, M. Julve, F. Lloret, J. Pasán, C. Ruiz-Pérez, Y. Journaux, *et al.*, "Highly selective chemical sensing in a luminescent nanoporous magnet," *Advanced Materials*, vol. 24, no. 41, pp. 5625–5629, 2012.

[13] Y. Cui, Y. Yue, G. Qian, and B. Chen, "Luminescent functional metal–organic frameworks," *Chemical reviews*, vol. 112, no. 2, pp. 1126–1162, 2011.

[14] R. Paschotta *et al.*, *Encyclopedia of laser physics and technology*, vol. 1. Wiley-vch Berlin, 2008.

[15] W. Koechner and M. Bass, *Solid-State Lasers: A Graduate Text*. Springer Science & Business Media, 2006.

[16] S. M. Abutarbush, "Saunders comprehensive veterinary dictionary," *The Canadian Veterinary Journal*, vol. 49, no. 9, p. 906, 2008.

[17] M. Allendorf, C. Bauer, R. Bhakta, and R. Houk, "Luminescent metal–organic frameworks," *Chemical Society Reviews*, vol. 38, no. 5, pp. 1330–1352, 2009.

[18] E. G. Moore, A. P. Samuel, and K. N. Raymond, "From antenna to assay: lessons learned in lanthanide luminescence," *Accounts of chemical research*, vol. 42, no. 4, pp. 542–552, 2009.

[19] N. Rakov, W. Lozano, E. L. Falcao-Filho, R. B. Guimarães, G. S. Maciel, and C. B. de Araújo, "Three-and four-photon excited upconversion luminescence in terbium doped lutetium silicate powders by femtosecond laser irradiation," *Optical Materials Express*, vol. 3, no. 11, pp. 1803–1809, 2013.

[20] B. Zhou, L. Tao, Y. H. Tsang, W. Jin, and E. Y.-B. Pun, "Super-broadband near-ir photoluminescence from pr 3+-doped fluorotellurite glasses," *Optics express*, vol. 20, no. 4, pp. 3803–3813, 2012.

[21] S. Das, H. Kim, and K. Kim, "Metathesis in single crystal: complete and reversible exchange of metal ions constituting the frameworks of metal- organic frameworks," *Journal of the American Chemical Society*, vol. 131, no. 11, pp. 3814–3815, 2009.

[22] Z. Wang and S. M. Cohen, "Postsynthetic covalent modification of a neutral metal- organic framework," *Journal of the American Chemical Society*, vol. 129, no. 41, pp. 12368–12369, 2007.

[23] O. S. Heavens and R. W. Ditchburn, *Insight into Optics*. Wiley and Sons, 1987.

[24] A. T. X. Products, "Supernova x-ray diffractometer system," *User manual*, vol. Version 1.9, 2014.

[25] G. M. Sheldrick, *SHELXL, SHELXS, Program for Crystal Structure Refinement*. Institute of Inorganic Chemistry, Tammannstrasse 4, D-37077 Göttingen, Germany.

[26] D. O. and P. H., *OLEX2: A complete structure solution, refinement and analysis program*, vol. 42. J. Appl. Cryst, 2009.

[27] K. Brandenburg and H. Putz, *DIAMOND, Crystal and Molecular Structure Visualization*. Crystal Impact GbR, Kreuzherrenstr. 102, 53227 Bonn, Germany, 1997-2016.

[28] J. Rodríguez-Carvajal and T. Roisnel, *FullProf.98 and WinPLOTR: New Windows 95/NT Applications for Diffraction Commission For Powder Diffraction*. International Union for Crystallography, 1998.

[29] OriginLab, *OriginPro 8*. Northampton, MA.